J. Fluid Mech. (1994), *vol.* 259, *pp.* 219–240

The role of coherent structures in bubble transport by turbulent shear flows

By K. J. SENE[1], J. C. R. HUNT[2] AND N. H. THOMAS[3]

[1] Institute of Hydrology, Wallingford, Oxfordshire OX10 8BB, UK

[2] Department of Applied Mathematics and Theoretical Physics, University of Cambridge, Silver Street, Cambridge CB3 9EW, UK *and* Meteorological Office, Bracknell, Berkshire RG12 2SZ, UK

[3] FAST Team, Chemical Engrg *and* FRED Ltd, Research Park, University of Birmingham, Edgbaston, Birmingham B15 2TT, UK

(Received 31 January 1989 and in revised form 2 August 1993)

Using Auton's force law for the unsteady motion of a spherical bubble in inhomogeneous unsteady flow, two key dimensionless groups are deduced which determine whether isolated vortices or shear-layer vortices can trap bubbles. These groups represent the ratio of inertial to buoyancy forces as a relaxation parameter $\Pi = \Delta U^2/2gx$ and a trapping parameter $\Gamma = \Delta U/V_T$ where ΔU is the velocity difference across the vortex or the shear layer, x is streamwise distance measured from the effective origin of the mixing layer and V_T is the terminal slip speed of the bubble or particle. It is shown here that whilst buoyancy and drag forces can lead to bubbles moving in closed orbits in the vortex flows (either free or forced), only inertial forces result in convergent trajectories. Bubbles converge on the downflow side of the vortex at a location that depends on the inertial and lift forces. It is important to note that the latter have been omitted from many earlier studies.

A discrete-vortex model is used to simulate the large-scale unsteady flows within horizontal and vertical mixing layers between streams with velocity difference ΔU. Trajectories of non-interacting small bubbles are computed using the general force law. In the horizontal mixing layer it is found that Γ needs to have a value of about 3 to trap about 50% of the bubbles if Π is about 0.5 and greater if Π is less. The pairing of vortices actually enhances their trapping of bubbles. In the vertical mixing layer bubbles are trapped mainly within the growing vortices but bubbles are concentrated on the downflow side of the vortices as Γ and Π increase. In a companion paper we show that lateral dispersion of bubbles can be approximately described by an advective diffusion equation with the diffusivity about equal to the eddy viscosity, i.e. rather less than the diffusivity of heat or other passive scalars.

1. Introduction

Observations of the motions of bubbles in air-entraining flows by Thomas (see Goldring, Mawer & Thomas 1980; also Thomas 1982) and in the wakes of bluff-body flows (Hulin, Fierfort & Coudol 1982) have revealed the phenomenon of bubbles travelling in discrete clusters within free shear layers. This behaviour (figure 1, taken from Goldring *et al.*) has been attributed to the presence of large-scale coherent eddies. In the present paper we seek to determine the influence of such coherent structures on the distributions of bubbles in free shear layers, using theoretical models and computer simulations. The plane coflowing turbulent mixing layer was chosen as a model field

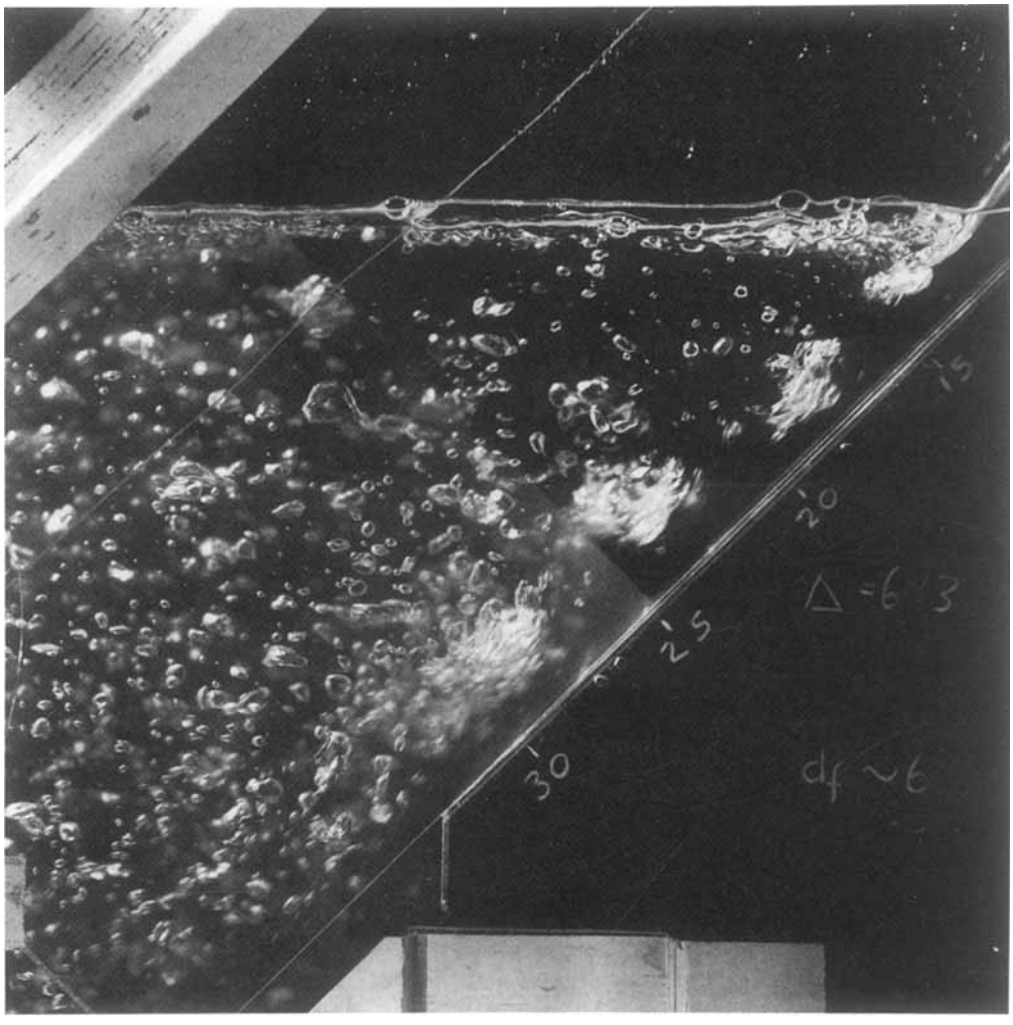

FIGURE 1. Photograph of air being carried underwater in the shear layer at the edge of a plunging jet. Depth of the jet about 2 cm; impact velocity about 2 m s^{-1}. (Photograph courtesy of Mr B. T. Goldring, CERL, Leatherhead.)

because of its advantages of simple geometry and extensive previous studies (e.g. Brown & Roshko 1974; Wood & Bradshaw 1982).

The physical mechanisms that lead to the trapping of bubbles by coherent structures can be explored by modelling the flow as a travelling vortex with a rotational core (see figure 2). This representation is suggested by visualizations of single-phase mixing layers (e.g. Brown & Roshko 1974) in which the coherent structures appear as roughly cylindrical blobs of rotational fluid connected by thin braids of turbulent fluid. The far-field flow induced by an isolated cored vortex approximates that induced by a line vortex. The motions of bubbles in the neighbourhood of a line vortex have been computed by Auton (1983), as first reported in Thomas *et al.* (1983), and later extended as described in Auton, Hunt & Prud'homme (1988). Following standard practice, Auton expressed the resultant force acting on a bubble as the sum of separate and uncoupled contributions from inertial effects (i.e. pressure gradient and added mass), buoyancy, drag and lift. He showed how entrapped bubbles spiral in towards the centre

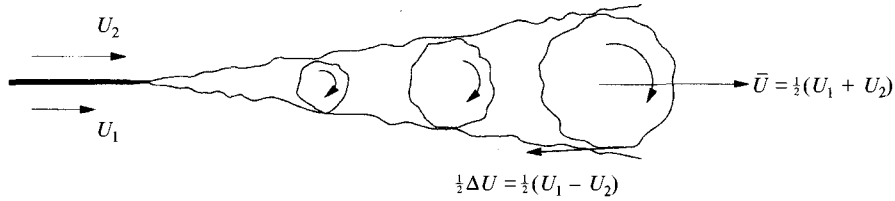

FIGURE 2. Sketch showing the representation of a two-stream planar mixing layer as a succession of travelling cored vortices.

of a line vortex as a result of the radial (centripetal) pressure gradient in the flow. In §2 we discuss the force law in detail and with particular reference to cored vortices akin to coherent structures in the turbulent mixing layer. Our hypothesis is that bubbles might be trapped in the radial pressure gradients which the coherent structures induce in the irrotational flow outside the mixing layer.

Once a bubble has entered a coherent structure it continues to move around under the influence of inertial, drag, buoyancy and lift forces. The motion may also be affected by other factors, such as the dispersive effects of small-scale turbulence carried within the structure and the pairing and tearing of the structures which has been observed in single-phase flows (e.g. Brown & Roshko 1974). It is necessary to understand the roles of these factors before we can make reliable estimates of the distributions of bubbles in turbulent mixing-layer flows.

Studies of the effects of drag, lift and inertial forces on the motion of bubbles in vortices have been made in connection with the transport of sand by the vortices shed from the crests of sand ripples (Tooby, Wicks & Isaacs 1977). Using a Rankine model of cored vortex flow (i.e. a circular disc of uniform vorticity), Tooby *et al.* showed that bubbles describe circular orbits as governed by a balance of drag and buoyancy forces. The effect of inertial forces is to cause bubbles to spiral in towards the centre of these circular orbits (Nielsen 1984; Sene 1985). In §§2 and 3 we develop these simple models in more detail as an aid to understanding qualitatively how inertial and turbulent dispersive forces affect the distribution of bubbles in mixing-layer vortices.

A more realistic representation of the evolving vorticity in the turbulent mixing layer can be achieved with the discrete-vortex modelling approach. This method is well established as a means of calculating large-scale unsteady aspects of free shear flows; see the review by Leonard (1980). It produces instantaneous patterns that look strikingly similar to those observed experimentally, including such features as the growth by pairing of clustered vorticity (i.e. coherent structures). Thus it seems most natural to apply this method to the study of discrete-phase dynamics in the mixing layer. Some preliminary results have already been presented by the authors in Thomas *et al.* (1983). Other workers have used the method to study the motions of particles in axisymmetric jets (Chein & Chung 1987; Chung & Troutt 1988), of passive contaminants in mixing layers (Thies & Peters, cited by Peters & Williams 1980) and of flame fronts in the lee of a backward-facing step (Ghoniem, Chorin & Oppenheim 1983). In §4 we describe how the method can be used in conjunction with the force law for bubble motion to estimate the effects of orientation with respect to gravity and of inertial and vorticity forces on bubbles in plane mixing layers. The results of the simulations appear in §5.

2. Theoretical considerations

2.1. *Equation of motion*

Auton's (1983) formulation of the equation of motion differs from previous work (e.g. Soo 1967; Wallis 1969) in that vorticity lift forces are incorporated and the added mass forces are represented correctly; see Thomas *et al.* (1983). The generalized force law, analysed and further justified by Auton *et al.* (1988), leads to the following equation of motion for bubbles:

$$\frac{\mathrm{d}\boldsymbol{v}}{\mathrm{d}t} = \frac{3\mathrm{D}\boldsymbol{u}}{\mathrm{D}t} - 2\boldsymbol{g} - 2g\left(\frac{\boldsymbol{w}}{V_T}\right) f\left(\frac{w}{V_T}\right) - 2C_L\, \boldsymbol{w} \times (\boldsymbol{\nabla} \times \boldsymbol{u}), \tag{1}$$

where $\boldsymbol{u}$ is the liquid velocity, $\boldsymbol{v}$ is the bubble velocity and $\boldsymbol{w} = \boldsymbol{v} - \boldsymbol{u}$ is the relative velocity, V_T is the rise speed in still water and C_L is the lift coefficient of the bubble in uniform shear; $C_L = 0.5$ for a spherical bubble (Auton 1983). The $\mathrm{D}/\mathrm{D}t$ operator denotes the total derivative following the liquid motions and the drag function $f(w/V_T)$ is assigned as described below.

The terms on the right-hand side of (1) represent the contributions to the bubble's acceleration from inertial forces (i.e. pressure gradient and added mass), buoyancy forces, drag forces and lift forces respectively. Several assumptions made in its derivation are discussed fully in Thomas *et al.* (1983). In summary, we believe (1) provides a sensible description of the most important forces affecting the motion of small spherical bubbles (up to 2 mm in diameter, say) at high Reynolds numbers based on V_T as representative slip speed in weakly inhomogeneous rotational flows. For simplicity of computations we have supposed a linear drag law (i.e. $f = 1$). Measurements (reviewed in Clift, Grace & Weber 1978) of the terminal speed of small bubbles about 2 mm in diameter rising through water show that V_T is about 20 cm s^{-1}, a value adopted throughout in our calculations. Sene (1985) has shown the results are not much affected by the particular choice of drag law provided that the same value of V_T is used.

2.2. *Limiting behaviour*

It is helpful to estimate the orders of magnitude of the various forces acting on a bubble travelling in a coherent structure. For a plane mixing layer with velocity difference ΔU and thickness δ at a distance x from its origin, the terms on the right-hand side of (1) have the following magnitudes (per unit mass of liquid):

$$\text{Inertia} \sim \Delta U^2/\delta; \quad \text{Buoyancy} \sim g; \quad \text{Drag} \sim gW/V_T; \quad \text{Lift} \sim C_L\, W(\Delta U/\delta),$$

where W is characteristic of the slip speed (see below). To understand the relative effects of these terms, it is convenient to introduce as parameters the inertia-to-buoyancy ratio (I/B), Π, and the lift-to-drag ratio (L/D), Π/Γ, where we define

$$\Pi = \Delta U^2/2gx. \tag{2a}$$

Here the factor 2 appears for convenience and δ has been assumed proportional to x as is appropriate for the turbulent plane mixing layer. Since the ratio of lift-to-drag forces is of order $\Delta U V_T/g\delta$, for convenience we choose the second independent parameter Γ to represent the ratio of rotational trapping velocities to the bubble rise velocity:

$$\Gamma = \Delta U/V_T. \tag{2b}$$

As we shall see, the parameter Γ effectively measures how well the vortex can trap

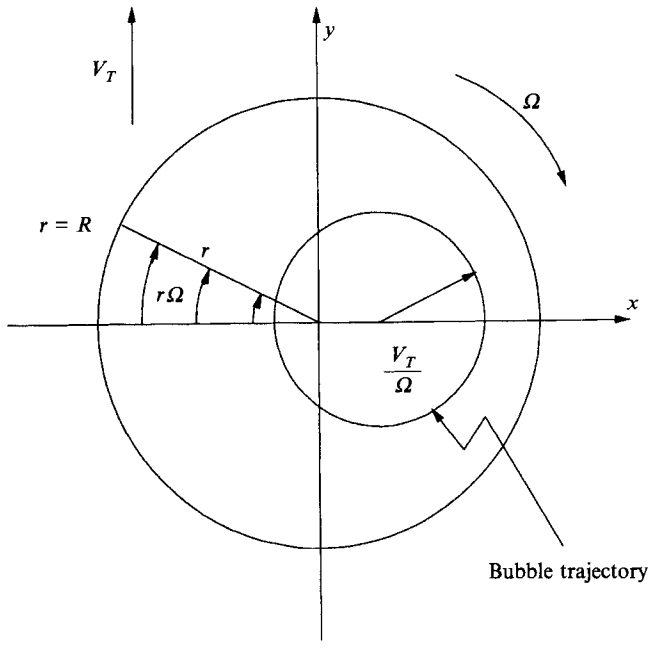

FIGURE 3. Sketch showing the trajectory of a bubble moving inside a Rankine vortex according to equation (4*b*).

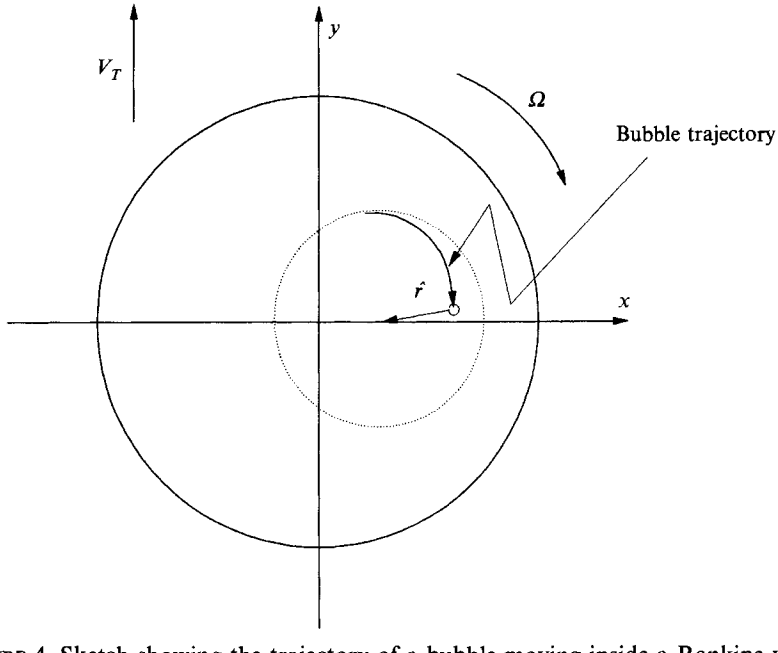

FIGURE 4. Sketch showing the trajectory of a bubble moving inside a Rankine vortex according to equation (5).

bubbles and hence it sets the magnitude of W in the vortex. If $\Gamma \ll 1$, there is no trapping and $W = V_T$. But if $\Gamma \gg 1$, then $W = \Delta U$, so that for strong shear (or small rise speed), the lift forces are then comparable with the inertial forces since $L/I \approx W\Delta U/\Delta U^2 \approx 1$. But if $\Gamma \ll 1$, then $L/I \sim V_T/\Delta U \approx 1/\Gamma \gg 1$, so for weak shear

layers, the lift force is then large compared with the inertial forces. On the other hand, it has a small effect because the bubbles slip quickly through the vortices.

When $\Pi \ll 1$ and $\Pi/\Gamma \ll 1$, both the inertial and lift forces are negligible compared with the buoyancy and drag forces and then (1) reduces to

$$\boldsymbol{v}-\boldsymbol{u} = \boldsymbol{w} \approx -V_T \boldsymbol{g}/g. \tag{3}$$

In this limit, the bubbles are transported as in a uniform flow of liquid at velocity $\boldsymbol{u}$.

3. First estimates of motions and concentrations

As a first approximation, coherent large eddies in a turbulent mixing layer can be represented as a succession of independent travelling cored vortices. Simplifying the picture in the interests of basic understanding, we begin by considering how bubbles move inside a single horizontal vortex of uniform section and vorticity Ω (i.e. a Rankine vortex). More realistic patterns and distributions of vorticity could be employed but the complexity of the analysis would mask the essential details. We then deduce the mean concentration profiles in mixing-layer flow, here assuming that the concentrations are so low that the bubble motions are sensibly independent of one another.

3.1. *Limit of small Π*

Consider first the limits $\Pi \to 0$ and $\Pi/\Gamma \to 0$. In this case, the local slip speed approximately equals the terminal rise speed and a bubble with vector coordinate $\boldsymbol{X}$ executes a circular motion defined by (with $C_L = \frac{1}{2}$)

$$\boldsymbol{v}^{(0)} = \mathrm{d}\boldsymbol{X}/\mathrm{d}t = -V_T \boldsymbol{g}/g - \boldsymbol{X} \times \boldsymbol{\Omega}, \tag{4a}$$

the solution for which is

$$\boldsymbol{X} = [\boldsymbol{X}_0 - (V_T/g\Omega^2)\boldsymbol{g} \times \boldsymbol{\Omega}]\cos(\Omega t) - \Omega^{-1}[\boldsymbol{X}_0 \times \boldsymbol{\Omega} + V_T \boldsymbol{g}/g]\sin(\Omega t) + (V_T/g\Omega^2)\boldsymbol{g} \times \boldsymbol{\Omega}, \tag{4b}$$

where $\boldsymbol{X}_0 = \boldsymbol{X}(t = 0)$. Equation (4*b*) defines a circular orbit located horizontally off-centre from the vortex axis at $V_T \boldsymbol{g} \times \boldsymbol{\Omega}/g\Omega^2$ (i.e. a distance V_T/Ω for a vortex with a horizontal axis; see figure 3). This result has been discussed and applied by Tooby *et al.* (1977).

If weak inertial and lift forces (i.e. such that $\Pi \ll 1$) are now considered to perturb this orbit with linearized perturbation velocity $\boldsymbol{v}^{(1)}$, then initially we have

$$\boldsymbol{v}^{(1)} = (V_T/g)[-\tfrac{3}{2}\Omega^2 \boldsymbol{r} + \tfrac{1}{2}\Omega^2 \hat{\boldsymbol{r}} - C_L(\boldsymbol{v}^{(0)} - \boldsymbol{u}) \times \boldsymbol{\Omega}], \tag{5}$$

where $\boldsymbol{r}$ is measured from the vortex centre and $\hat{\boldsymbol{r}}$ from the orbit centre. If initially $r > V_T/\Omega$, the particle slowly drifts towards the centre of the vortex because the radial pressure gradient (the term in $\boldsymbol{r}$ in (5)) is larger than the centrifugal acceleration (the term in $\hat{\boldsymbol{r}}$) and the lift term which acts horizontally; see figure 4. These terms become comparable when the radius of the orbit is of the same order as the orbit displacement, i.e. when $r = V_T/\Omega$. Eventually the bubbles converge to an equilibrium location where there is a balance of the horizontal lift force $C_L V_T(\boldsymbol{g}/g) \times \boldsymbol{\Omega}$ and the radial acceleration $\frac{3}{2}\Omega^2 \boldsymbol{r}$. This equilibrium position is defined by

$$\boldsymbol{r}_e = \tfrac{2}{3} C_L (V_T/g\Omega^2)\boldsymbol{g} \times \boldsymbol{\Omega}. \tag{6a}$$

For a horizontal vortex, then,

$$r_e \approx 0.3 V_T/\Omega \tag{6b}$$

on the downflow side. Note that this equilibrium point is defined independently of the relative strength of the inertia-to-buoyancy forces Π, provided that the vortex is just strong enough to trap the particles, i.e. $\Gamma > 1$. Note also that the location of this point does not depend on the drag law but it does depend on the value of the lift coefficient. This conclusion differs from that obtained by Nielsen (1984) who ignored the lift force and based his calculations on an incorrect expression for the added mass.

3.2. *Limit of large* Π

It is also worthwhile to consider the case where the bubble moves entirely under the action of inertial and lift forces in the vortex flows, with the buoyancy and drag forces being negligible, i.e. when $\Pi \to \infty$. Then, from (1),

$$\mathrm{d}\boldsymbol{v}/\mathrm{d}t = -3\Omega^2 \boldsymbol{r} - 2C_L(\boldsymbol{v} - \boldsymbol{r} \times \boldsymbol{\Omega}) \times \boldsymbol{\Omega}. \tag{7a}$$

Therefore in this limit too the radial pressure gradient encourages bubbles to travel towards the centre of the vortex. There is only an equilibrium position at the vortex centre if the bubble is placed there with zero velocity. If the bubble is released anywhere else it does not reach the centre of the vortex but executes oscillations. This limit is not really of much practical interest.

3.3. *Limit of small* Π *and large* Γ

The outer part of a coherent structure is similar to the outer free vortex zone of a Rankine vortex. Auton (1983) has shown that when bubbles are released in the vicinity of a free vortex of circulation κ, there is a single trajectory (of maximum radius κ/V_T) on which the bubbles can move in a closed orbit in the limit $\Pi \to 0$ and $\Pi/\Gamma \to 0$. In general, bubbles are trapped in vortices if they are released inside a certain width which, for weak vortices, is proportional to the ratio κ/V_T. Thus a Rankine vortex possessing core radius R_0 can only trap bubbles if $\kappa/2\pi R_0 > V_T$, that is if the maximum vortex flow speed $U_M > V_T$, equivalent to $\Gamma > 1$.

We can now conjecture that in a typical coherent structure with $U_M \sim \frac{1}{2}\Delta U$, the bubbles are trapped if $U_M > V_T$. When trapped, they move on circular trajectories, concentrating on the downflowing side at a distance between 0.3 and 1.0 times $V_T R/U_M$ from the centre of the structure. This corresponds to the high-speed side in a downflowing free shear layer when, since $R \approx \frac{1}{2}\delta$ and $\delta \approx bx$ (where b is the spread rate coefficient), the accumulation locus of the bubbles is approximately $r/x = bV_T/\Delta U$.

3.4. *Incorporating turbulent dispersion*

This aspect will be considered in detail in a companion paper (Sene, Thomas & Hunt 1993). For completeness of the present account we mention here key points in the representative case with $\Pi \ll 1$, when the radial convergence velocity of bubbles towards the centre of a coherent structure is given by

$$\frac{\mathrm{d}r}{\mathrm{d}t} = -U_{pr} \quad \text{with positive} \quad U_{pr} \propto \frac{V_T}{g}\frac{\Delta U^2}{\delta^2} r \propto V_T \Pi \frac{r}{x}. \tag{7b}$$

In a real coherent structure, this radially inwards motion would be opposed by the outwards dispersive effects of small-scale turbulence. Current ideas about the dynamics, as reviewed by Hussain (1983), are that the intensities rise to a peak near the centre and

drop to a small value at the edge, such that contours of turbulence intensity are roughly symmetric about the centre. Consistent with these results, we might represent their effects on the motions of small bubbles by a diffusion coefficient K_{pr}, say, whose local distribution depends only on radial position inside the coherent structure. Thus, with $\delta \propto x$, we can write

$$K_{pr}/\Delta U = xh(r/x), \tag{8}$$

where h is some (unknown) function of r/x. The bubble concentration C_T, say, inside the coherent structure is then given by

$$U_{pr} C_T = K_{pr} \partial C_T/\partial r. \tag{9}$$

With $C_T(0) = C_{T0}$, substitution of (7*b*) and (8) in (9) gives

$$\ln\left(\frac{C_{T0}}{C_T}\right) \propto \frac{\Pi}{\Gamma}\int_0^{\mu} \frac{\mu'}{h(\mu')} \mathrm{d}\mu', \tag{10}$$

where $\mu = r/x$ and a prime denotes a dummy variable of integration. This result indicates that bubble concentrations inside a coherent structure are increasingly confined as Π/Γ increases. However, in view of the declared restrictions on our bubble dynamic model and of the acknowledged limitations in diffusivity modelling of turbulent dispersion, this finding is probably best regarded as no more than a scaling guideline.

The concentrations given by (10) can be related to the concentrations in an Eulerian frame of reference by means of an intermittency function $\bar{\gamma} = \bar{\gamma}(\eta)$, where η is the mixing-layer similarity variable y/x (e.g. Townsend 1976). This method of relating Lagrangian to Eulerian results has been used previously by Fiedler (1974). The intermittency distribution is defined by instantaneous $\gamma = 1$ in turbulent fluid and $\gamma = 0$ in non-turbulent fluid; the bar denotes statistical averaging. Measurements of the intermittency distribution across turbulent mixing layers (e.g. Fiedler 1974) suggest that

$$\gamma(\eta) = \exp(-P\eta^2), \tag{11a}$$

where P is a constant. Bubble concentrations C in an Eulerian frame are then given by

$$C/C_0 = \gamma C_T/C_{T0}. \tag{11b}$$

Inspection of (9) and (10) shows that the main findings about the form of the C_T-profiles should then apply equally to the C-profiles.

4. Computer simulations

We now describe our method for calculating ensemble tracks of bubbles in the mixing layer simulated by a discrete-vortex method, using (1) to represent the motions of the bubbles. It is assumed that the bubbles are small enough and in low enough concentrations that they do not affect the flow or each other. The discrete-vortex algorithm used here is described in §4.1. The main output from these calculations is the vorticity distribution of the flow in discrete form. Section 4.2 describes our procedure for generating and smoothing this spotty flow field so as to recover sensible estimates of the velocity gradients for use with the bubble dynamic equation (1). The flow-field results appearing in §4.3 are then applied to calculations of the bubble transport as described in §4.4.

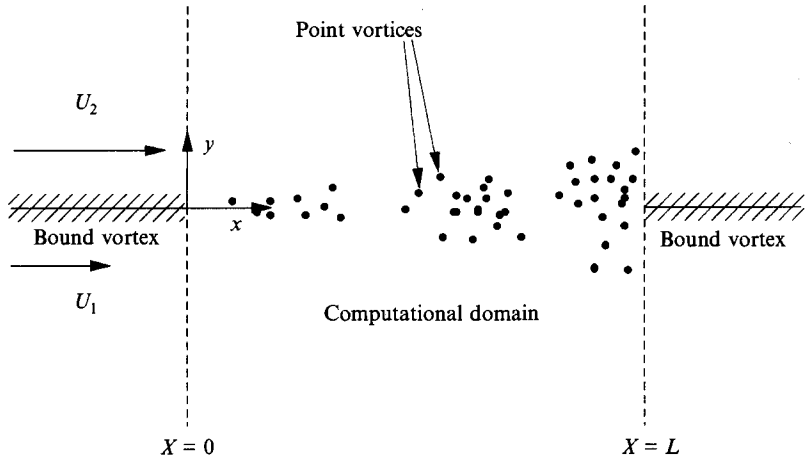

FIGURE 5. Definition sketch for discrete-vortex simulation of a two-stream planar mixing layer.

4.1. *Mixing-layer flow*

Many different formulations of the discrete-vortex method have been proposed (e.g. see the review by Leonard 1980) and recent developments (e.g. Ashurst & Meiburg 1988) have even extended to simulations of the three-dimensional eddy structure in plane shear flows. However, for the present purpose of demonstrating key basic features of bubble transport by large eddies, we employ the simpler two-dimensional representation essentially as described by Ashurst (1977) but incorporating a vortex-in-cell scheme (Spalart & Leonard 1981) to reduce computational overheads.

Important features of the model are sketched in figure 5: note that the flow is assumed to be inviscid and two-dimensional. The vorticity shed from the origin of the mixing layer ($x = 0$) is represented in discrete form by a sequence of point vortices. The strength of each point vortex is chosen to be $\Delta\kappa = \Delta U\,\bar{U}\,\Delta t$, where Δt is the time step; this reproduces the correct vorticity influx to the mixing layer. The point vortices move under the influence of the mean velocity field $\bar{U}$ and the velocity field induced by all the other point vortices in the flow. Point vortices are removed from the flow at the downstream end of the computational domain ($x = L$) chosen so as to limit the total number of vortices and hence the computational time required. The exiting vortices in $x > L$ and the attached sheet on the splitter plate in $x < 0$ are both represented as bound vorticity. Following Leonard (1980), the simulation is started by placing the downstream bound vortex at $x = 0$ and then moving it downstream at a velocity $\bar{U}$ until it reaches the chosen location of $x = L$. The simulation is advanced at each time step by a simple Euler predictive scheme $\boldsymbol{x}_{n+1} = \boldsymbol{x}_n + \boldsymbol{u}_n \Delta t$. Vortices are released into the flow at the position $x = L/\bar{N}$, where $\bar{N}$ is the average number of vortices in the simulation. Note that the boundary conditions on the splitter plate in $x < 0$ are not satisfied correctly, nor is the vorticity downstream of $x = L$ represented correctly, so the simulation is only approximately valid in the computational domain $0 < x < L$.

4.2. *Numerical considerations*

The discrete-vortex method may provide a formal solution to the Euler equations in the limit $\bar{N} \to \infty$ although this is still a moot point: see Moore (1981). However, as posed, the model is inherently unstable and overpredicts the turbulence intensities. Also, an inordinate amount of computer time is needed to attain stationary statistics.

Several *ad hoc* devices are available to overcome these problems, as discussed below. Their only justification is pragmatism – namely, for the purpose of calculating the bubble trajectories, it suffices to use a flow field that sufficiently resembles the real turbulent mixing layer, without necessarily being an exact solution of the flow equations.

Numerical instabilities arise because the induced velocity is singular at the centre of each point vortex. This produces unrealistic results when vortices approach each other too closely and are expelled at high velocity from the computational domain. Such behaviour can be suppressed by including a finite core size in each vortex (Chorin 1973). Chorin's device is employed here and the core model used is $u_\theta = \frac{1}{2}\Delta U$ on $r = r_c$, where r_c is the core radius and u_θ is the spin component velocity. The radius r_c is taken arbitrarily as $0.5L/\bar{N}$. More complicated core models may be justified heuristically but they do not appear to systematically improve the calculated flow field (Leonard 1980).

A plausible reason for the overprediction of turbulent intensities by the discrete-vortex model is that, being two-dimensional, the method does not represent energy transfer into the third component, either as large-scale motion or as fine-scale turbulent scrambling. Ashurst & Meiburg (1988) have explicitly studied this effect in modelling the plane mixing layer as a collection of vortex filaments. In the present two-dimensional simulations, artificial diffusion is used to mitigate this deficiency. The diffusion is included as a Gaussian random jitter on the motion of each vortex, according to the following time-stepping scheme:

$$\boldsymbol{x}_{n+1} = \boldsymbol{x}_n + \boldsymbol{u}_n \Delta t + \boldsymbol{\zeta},$$

where $\boldsymbol{\zeta}$ is the (isotropic) vector jitter with standard deviation ζ' expressed here as a fraction of the average distance moved by each vortex in each time step – that is, $\zeta' = \epsilon \bar{U} \Delta t$. The effect of the modelling coefficient ϵ on the results of a mixing-layer simulation were investigated by Kiya, Arie & Harigane (1980), using 100 vortices in the computational domain. Close agreement with measured values of the turbulent intensities was obtained only for such large values of ϵ, i.e. $\epsilon \sim 1$, that the jitter completely obliterated the coherent structures. In the present simulations, lower values of ϵ were used in order to retain the structural features.

The time required for a simulation increases as $\bar{N}^2$ which, in practice, imposes a serious constraint on the number of vortices that can be used in the simulation. Computing times were reduced in the present calculations by an approximate scheme based on the work of Spalart & Leonard (1981). According to this algorithm, a mesh is superimposed on the computational domain so that each vortex can be assigned to a cell at each time step (figure 6*a*). The velocity induced by vortex interactions for a separation distance x_a, say, is then expanded as a Taylor series in the separation distance x_b between the cells in which the vortices are located. Errors are limited by taking sufficient numbers of terms in the Taylor series. In the present work, a simpler scheme was found to be satisfactory; see figure 6(*b*). Interactions between vortices in the same cell and adjoining cells are computed exactly but all other interactions are calculated as if the vortices were located at the centres of their cells. For a cell size δ, the maximum error in estimated velocity due to any one interaction is of order $\Delta\kappa/2\pi\delta$, so the position error at the next time step is then of order $\Delta\kappa\Delta t/2\pi\delta$. In practice, provided that the cells are small compared with the coherent structures, these errors tend to cancel because the vortices are essentially randomly distributed within the cells. Also, the error term is always very much less than the imposed random jitter ζ'.

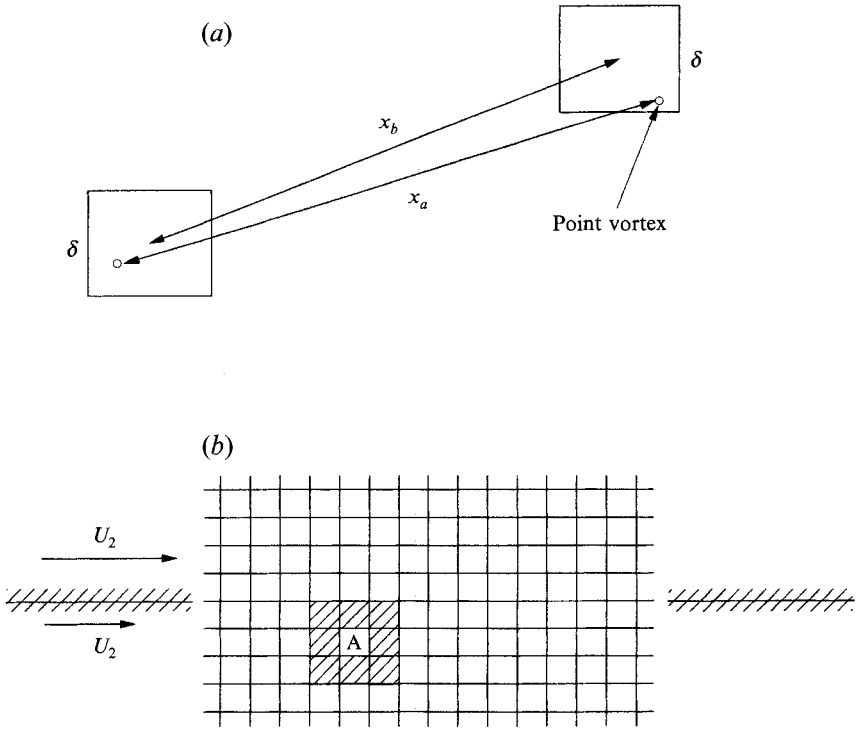

FIGURE 6. Approximate schemes for calculating point-vortex interactions: (*a*) Scheme of Spalart & Leonard (1981); (*b*) scheme used in the present study. In (*b*) the interactions between the vortices in cell A and those in the shaded cells are calculated exactly and the remainder are calculated approximately.

The approximate scheme for computing vortex interactions was tested in a 320-vortex simulation of a single-stream mixing layer. Vortex positions and the time-averaged velocity field were calculated using both the exact and the approximate schemes. There was little difference between the results but the exact scheme required about 2 s of run time whereas the approximate scheme took about 0.4 s to advance the simulation by one time step on the University of Cambridge IBM 3081 computer. The cell size was arbitrarily set to $0.05L$ and further reductions in run time could have been achieved by optimizing the cell size.

4.3. *Flow-field calculations*

A two-stream mixing layer with velocity ratio $U_2/U_1 = 3$ was chosen for this test so as to match the conditions of the experimental study described in Sene *et al.* (1993). The average number of vortices in the simulation domain was chosen to be about 500. The cell size used was $0.016L$ (optimized on minimum runtime) with two jitter values: $\zeta' = 0.2\bar{U}\Delta t$ and $0.4\bar{U}\Delta t$. Each simulation was run for 5000 time steps. A sequence of the vortex positions at time intervals of $0.2L/\Delta U$ is shown on figure 7 for the simulation with jitter $\zeta' = 0.4\bar{U}\Delta t$. The vortices cluster into groups that closely resemble the coherent structures observed in turbulent mixing layers. The density of these vortex distributions gives a qualitative idea of the vorticity concentrations in the large features.

Mean velocities calculated from this simulation are shown in figure 8(*a*). Measurements by Wood & Bradshaw (1982) show that the mixing-layer width, defined

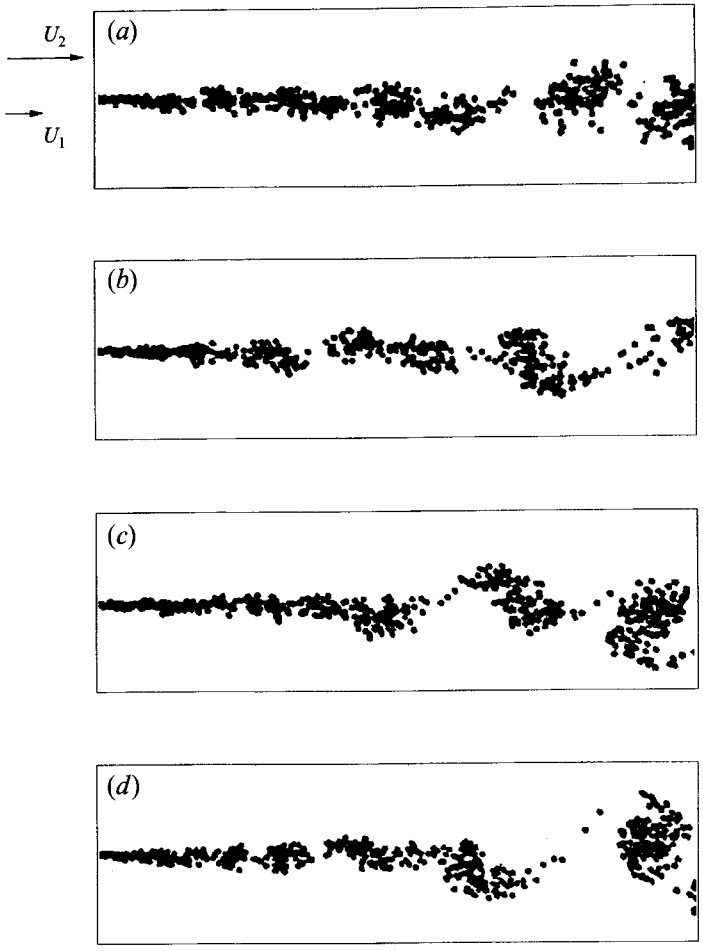

FIGURE 7. Positions of point vortices in the discrete vortex simulation of a two-stream planar mixing layer at times: (*a*) $2.2L/\Delta U$; (*b*) $2.4L/\Delta U$; (*c*) $2.6L/\Delta U$; (*d*) $2.8L/\Delta U$.

as the distance between the points at which the velocity differs by 0.5% from the stream value, is about $0.22x$ for single-stream layers. Since the width also scales in proportion to the ratio $\Delta U/\bar{U}$ (Townsend 1976), a mixing layer with velocity ratio of 3 would be expected to spread as $0.11x$, approximately. Our simulations with $0.14x$ slightly overpredict this value, although not by much more than the typical uncertainty of $\pm 20\%$.

The shapes of the turbulence intensity profiles appearing in figures 8(*b*) and 8(*c*) are in reasonable agreement with experimental measurements (e.g. Wood & Bradshaw 1982). The latter show peak values of the r.m.s. u' and v' components that are about 0.18 and 0.14 of the shear velocity ΔU, irrespective of the velocity ratio. The peak value of the Reynolds shear stress $\overline{u'v'}$ is about $0.013\Delta U^2$ according to measurements and this value, like the peak r.m.s. u', is reproduced rather well by the calculations; see figure 8(*d*). However, the peak r.m.s. v' is overestimated by about 30% with r.m.s. jitter $\zeta' = 0.4\bar{U}\Delta t$, a mismatch that increased the r.m.s. jitter was halved. For this reason, we fixed the jitter coefficient at 0.4 for all subsequent calculations of the bubble transport.

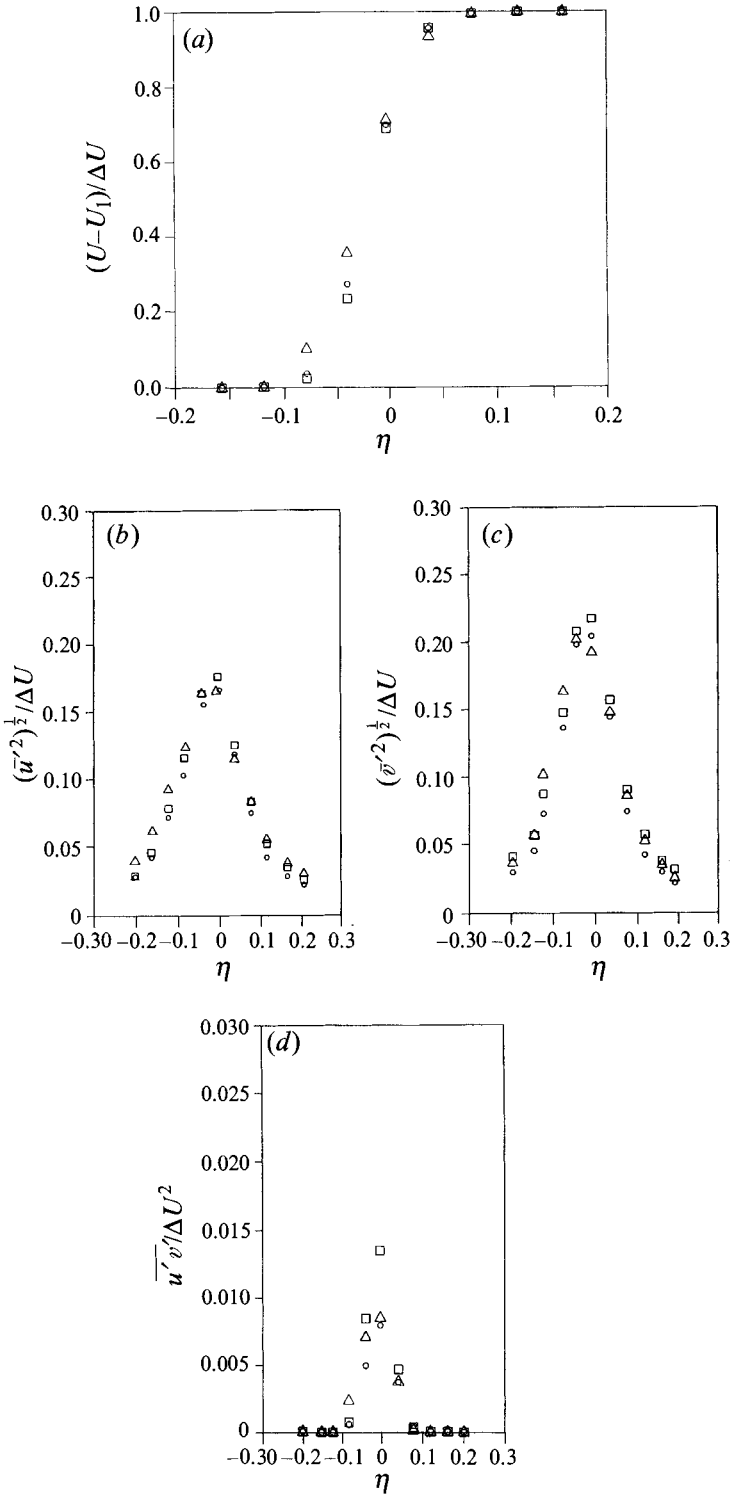

FIGURE 8. Mean velocities and turbulence intensities calculated over the duration of the discrete-vortex simulation: △, $x = 0.25L$; ○, $x = 0.50L$; □, $x = 0.75L$. (*a*) Mean velocity; (*b*) r.m.s. u'; (*c*) r.m.s. v'; (*d*) shear stress.

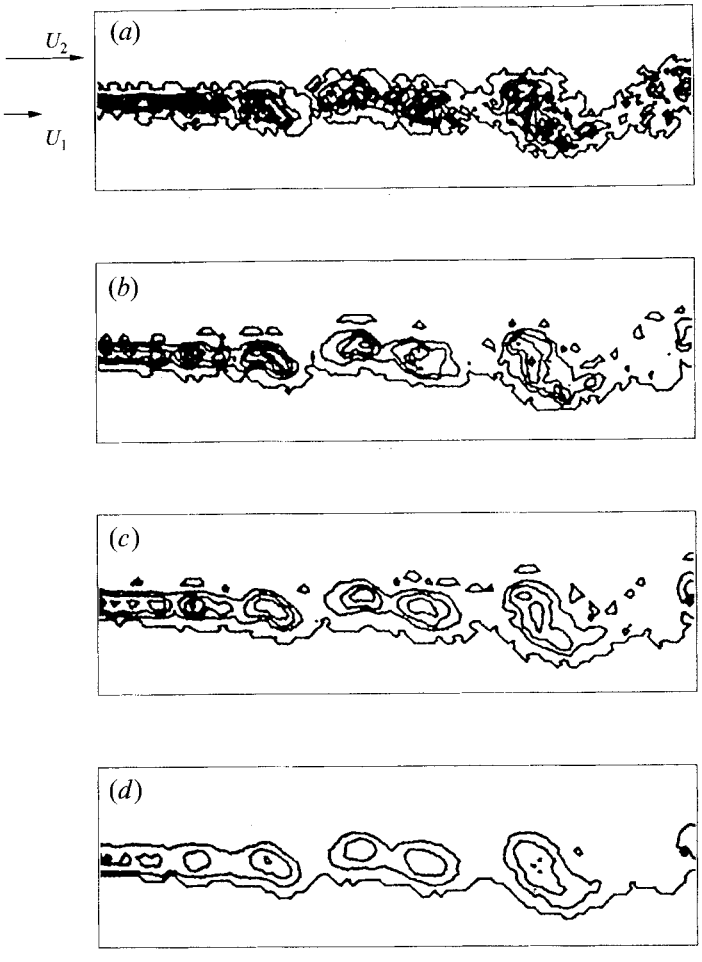

FIGURE 9. Vorticity distribution in the discrete-vortex simulation at time $2.4L/\Delta U$: (a) $\Delta x_0 = 1.75\bar{U}\Delta t$; (b) $\Delta x_0 = 3.50\bar{U}\Delta t$; (c) $\Delta x_0 = 5.00\bar{U}\Delta t$; (d) $\Delta x_0 = 7.50\bar{U}\Delta t$.

4.4. *Calculations of bubble motion*

The single-phase simulations, developed as described above to provide a reasonable compromise between retention of large structure features and reproduction of measured values of the statistical properties, were used for all the bubble calculations reported here. For the computational work, it proved convenient to scale all velocities on the shear velocity ΔU and all lengths on L, the length of the computational domain. The resulting dimensionless version of (1) governing the bubble dynamics is then

$$\mathrm{d}\tilde{\boldsymbol{v}}/\mathrm{d}\tilde{t} = 3\mathrm{D}\tilde{\boldsymbol{u}}/\mathrm{D}\tilde{t} - \Pi^{-1}[\boldsymbol{g}/g - \Gamma(\tilde{\boldsymbol{v}} - \tilde{\boldsymbol{u}})] - 2C_L(\tilde{\boldsymbol{v}} - \tilde{\boldsymbol{u}}) \times (\boldsymbol{\nabla} \times \tilde{\boldsymbol{u}}), \tag{12}$$

where $\tilde{\boldsymbol{v}} = \boldsymbol{v}/\Delta U$, $\tilde{\boldsymbol{u}} = \boldsymbol{u}/\Delta U$ and $\tilde{t} = t\Delta U/L$. The two parameters $V_T/\Delta U$ and $\Delta U^2/2gL$ (i.e. $1/\Gamma$ and Π) must be specified before (12) can be evaluated. The velocity $\boldsymbol{u}$ and the spatial gradients $\boldsymbol{u}\cdot\boldsymbol{\nabla}\boldsymbol{u}$ and $\boldsymbol{\nabla}\times\boldsymbol{u}$ are estimated from the discrete-vortex simulations. The latter values were initially calculated from analytical expressions for the vortex-induced velocity fields but these estimates were found unsatisfactory because of unrealistically large excursions associated with individual vortices. The difficulty is illustrated by figure 7: whilst the vortices label the large-scale structures, they do not give a realistic representation of the approximately uniform vorticity

within the structures. To eliminate this difficulty, the gradients were smoothed via a curve fit to the velocities at several nearby points, the latter obtained from averaging over a few time steps prior to the fitting. Thus the time step used for the bubble calculations (Δt_b say) exceeded that used for the mixing-layer simulations. The curve fitting procedure and the size of the time step Δt_b were developed from a model problem of bubble transport in a Rankine vortex. The velocity gradients, including those for vorticity, and the bubble trajectories in the Rankine vortex (see §3) were calculated analytically and then compared with the results of discrete vortex calculations using several numerical smoothing schemes (as described in Sene 1985). The following method was found to be the most satisfactory and was adopted for all the bubble calculations reported here.

Derivatives of the velocity at a point x_0 (say) were estimated by fitting a least-squares line to the velocities (averaged over Δt_b) at the points $x_0 + n\Delta x_0$, where integer n runs from -2 to $+2$. An appropriate value for Δx_0 was determined from an examination of the field smoothing of vorticity obtained with this algorithm. Figure 9 shows the vorticity distributions at a time $T = 2.4L/\Delta U$ for several different values of Δx_0. The detailed structure relating to individual vortices can be distinguished at the lowest value of $\Delta x_0 = 1.75\bar{U}\Delta t$ but this is progressively removed as Δx_0 is increased. Notice that for all the values of Δx_0 shown here, the main features of the vorticity distributions are strikingly similar to those observed experimentally (Wygnanski & Weisbrot 1988). Indeed, peak values of vorticity in the coherent structures (Hussain 1983) are roughly twice the maximum value of the mean velocity gradient $\partial u/\partial y$ and this ratio is recovered when $\Delta x_0 = 5\bar{U}\Delta t$ is selected. Accordingly, a filter coefficient of 5 was adopted for all subsequent calculations. Consistent with this tuning, the bubble time-step coefficient was also set to 5 (i.e. $\Delta t_b = \Delta x_0/\bar{U}$ strictly as appropriate for equilibrium transport) in all of the subsequent calculations. The time derivatives of the velocity field were estimated in the same way: $\partial \boldsymbol{u}/\partial t$ was assigned by least-squares fitting the velocity record at a fixed point over the time interval Δt_b (i.e. five-point smoothing).

5. Results

Several important aspects were simulated, as follows.

(*a*) The effects of velocity difference across the shear layer on the escape of bubbles from horizontal flow. Recall that the single-vortex model of §3 suggested that trapping occurs if $\Gamma = \Delta U/V_T > 2$ and that trapping is intensified by the action of inertia forces.

(*b*) The effects of pairing of coherent structures (as is observed experimentally, e.g. Brown & Roshko 1974) on the escape of bubbles from horizontal flow. Our preconception was that the flow disruption during pairing might encourage the escape of bubbles from the mixing layer.

(*c*) The effects of inertial forces on the distribution of bubbles in vertical downflows. Recall that the single-vortex model of §3 suggested that inertial forces cause the bubbles to drift toward the high-speed side of the mixing layer in downflow. Vertical downflow was adopted because buoyant slip of the bubbles is partially countered by the opposing flow, thereby affording simplifications both in the interpretation of the simulations and in their experimental realization.

For all of the results described below the model bubbles were released with initial velocity equal to the vector sum of the local flow and the bubble rise velocities.

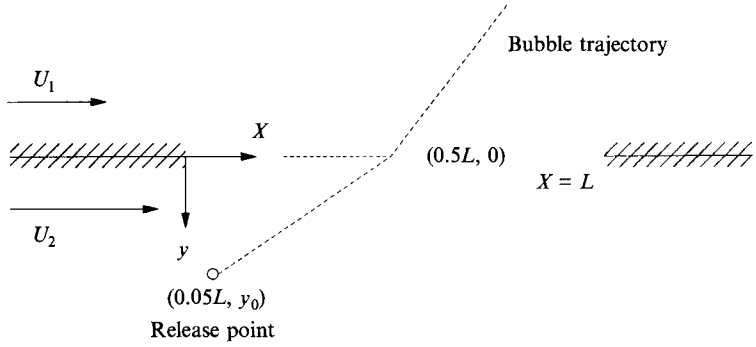

FIGURE 10. Sketch showing how the release point was calculated for use in the simulations. The dotted line shows the trajectory that a bubble rising at velocity V_T would follow in the absence of the mixing layer.

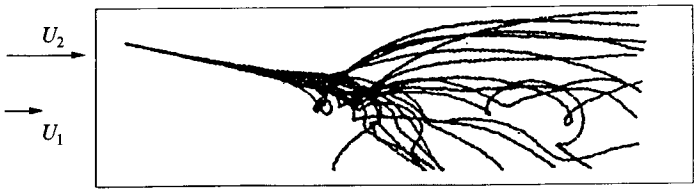

FIGURE 11. Simulation of bubble trajectories in a horizontal mixing layer. 20 bubbles with $\Pi = 0.5$, $\Gamma = 3.3$. (Note: gravity acts upwards here.)

5.1. *Escape of bubbles from a horizontal mixing layer*

The bubbles were introduced into the flow at coordinate $(0.05L, y_0)$ with a time interval of $200\Delta t$ between each bubble. The value of y_0 was selected such that the bubbles would travel through the point $(0.5L, 0)$ in the absence of the mixing layer, i.e. due to advection and slip. The determination of y_0 is portrayed on figure 10. Having y_0 as a parameter allows direct comparison of the results for different values of Γ since the bubbles then experience similar velocity histories whilst travelling in the mixing layer.

Figure 11 shows the bubble trajectories when $\Pi = 0.5$ and $\Gamma = 3.3$. Notice that gravity is directed upwards here so the bubbles are rising towards the bottom of this picture! Viewed in a fixed frame, these trajectories follow cycloidal paths within the coherent structures. In this simulation approximately half the bubbles were entrained into the mixing layer and remained trapped throughout the computational domain. The escape probability P is thus about 0.5 here. The dependence of P on Π and Γ is displayed on figure 12 where each data point represents expectations based on the histories of 20 bubbles. These results show that high values of Π inhibit escape, consistent with physical expectations of inertial confinement. Similarly, increasing values of Γ discourage escape, again as expected.

Bubbles appear to have zero probability of escape when $1/\Gamma = V_T/\Delta U$ is less than about 0.05, irrespective of Π. This result can be attributed to the downstream spread of the mixing layer, the time-averaged edge of which has locus $y/x \approx \pm 0.07$ in our simulations, so bubbles cannot escape when $V_T/U_1 < 0.07$, or $V_T/\Delta U < 0.035$ here (with $\Delta U/U_1 = 2$), a condition not far removed from that found with the simulations.

The conditions for which $P = 0.5$ can be adopted as a measure of criticality for trapping. From figure 12 we see that this parameterization yields critical values of $1/\Gamma = 0.11$, 0.19 and 0.30 when $\Pi = 0$, 0.05 and 0.50. These results might be compared with measurements by Shibiyama & Horikawa (1980) of sand-grain trapping in vortices. They found that the maximum velocity (U_m, say) induced by sand-ripple

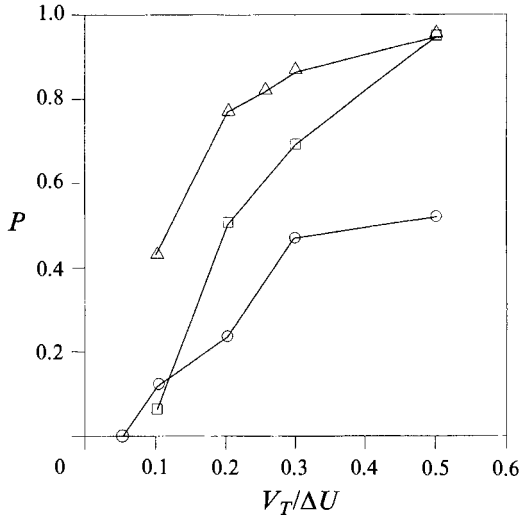

FIGURE 12. Calculations of the probability of bubbles escaping from a horizontal mixing layer: △, $\Pi = 0$; □, $\Pi = 0.05$; ○, $\Pi = 0.5$.

vortices occurs close to the bed. All sand grains were observed to be trapped when $V_T/U_m < 0.15$ and none when $V_T/U_m > 0.25$, where V_T here is the terminal fall speed of the grains. With our parameterization above, this corresponds to a critical condition somewhere in the interval 0.15 and 0.25. Supposing that U_m corresponds roughly to $\frac{1}{2}\Delta U$, their trapping condition then relates to $1/\Gamma$ between 0.075 and 0.125, as compared with our finding (for bubbles in a plane mixing layer) that $P = 0.5$ when $1/\Gamma$ is about 0.11; we take $\Pi = 0$ since inertial effects are not significant for sand-grain motions (Nielsen 1984). Thus there does seem to be similarity between the conditions for trapping in these two flows.

5.2. *Effects of coherent-structure pairing*

We expected that flow disruption during pairing events would encourage the release of bubbles. Two simulations were run to look at this aspect with the aid of the pairing event displayed on figure 7. Values of $\Pi = 0.5$ and $1/\Gamma = 0.1$ were chosen for the first simulation and $\Pi = 0$ and $1/\Gamma = 0.2$ for the second. In each simulation, fifteen bubbles were introduced along the line $y = 0.02L$, directly below the two eddies participating in the event.

The results are displayed in figure 13. Bubble locations are shown at times corresponding to the vortex position pictures of figure 7. Again we caution that gravity is directed upwards in these figures. What this test establishes is that there is little evidence of pairing having any significant effects on the trapping behaviour. We found $P = 0.07$ and $P = 0.60$ respectively in the two simulations, values that correspond closely with those obtained for the long-term (i.e. undiscriminated) expectations; see figure 12. The reason is probably that the contours of vorticity, although distorted, persist throughout the pairing event, so the local flows resemble those of a growing isolated eddy with closed, roughly circular, streamlines.

A striking feature of the simulation with $\Pi = 0.5$ is the pronounced clustering of bubbles within the eddies, demonstrating the trapping effect of inertial forces. Contrast this behaviour with that of the case $\Pi = 0$, shown in figure 13(*b*). Our findings here are consistent with those obtained from the isolated-vortex model described in §3. More detailed consideration is given to this behaviour in the following section.

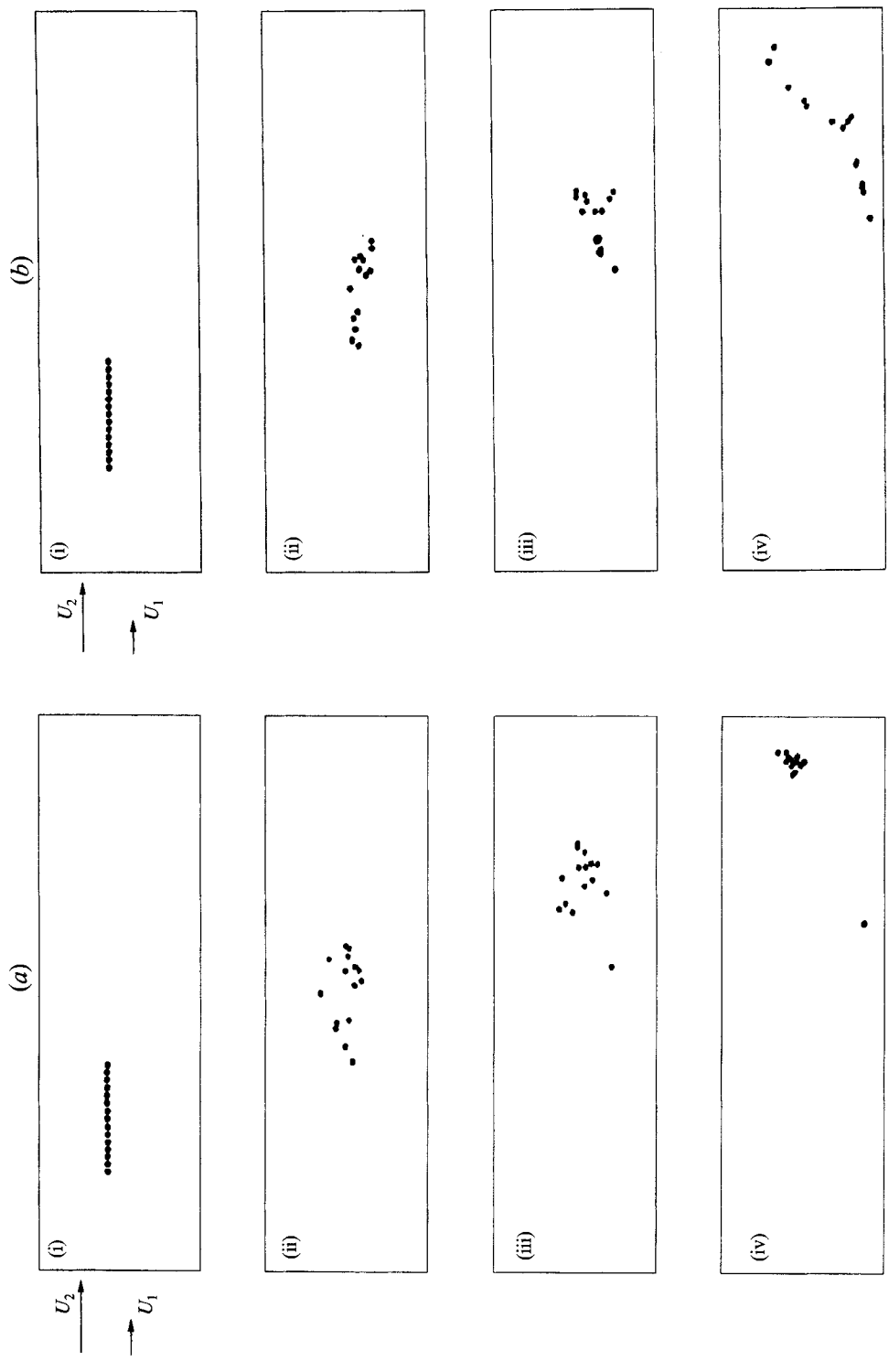

FIGURE 13. Simulations of bubble motion through two coherent structures undergoing a pairing: (*a*) $\Pi = 0.5$, $\Gamma = 10$; (*b*) $\Pi = 0$, $\Gamma = 5$. (Note: gravity acts upwards here.) Frames (i)–(iv) correspond to (*a*)–(*d*) in figure 7.

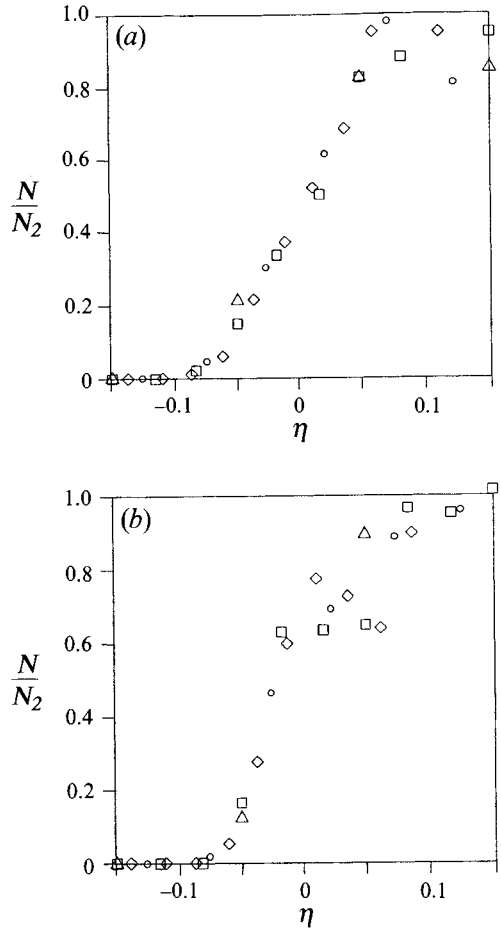

FIGURE 14. Calculations of bubble concentration fluxes in a vertical downflowing mixing layer. $N_2 (= 40)$ bubbles were released into the high-speed stream in the region $0 < y < 0.135$: (*a*) $\Pi = 0$, $\Gamma = 5$; (*b*) $\Pi = 0.067$, $\Gamma = 5$. △, $x = 0.2L$; ○, $x = 0.4L$; □, $x = 0.6L$; ◇, $x = 0.8L$.

5.3. *Bubble distributions in vertical downflows*

The model bubbles were introduced into the high-speed stream close to the origin of the mixing layer, in particular along the line $x = 0.05L$ and at random locations $0 < y_0 < 0.135L$. The time step here was $100\Delta t$ and groups of ten bubbles were followed in each of two simulations, both with $1/\Gamma = 0.2$, the first having $\Pi = 0$ (zero inertial forces) and the second $\Pi = 0.067$, corresponding to the conditions of our experimental study (Sene *et al.* 1993). A total of 360 bubbles was tracked in each simulation, requiring about 20 minutes of computing time for the case $\Pi = 0$ and about 2 hours for the case $\Pi = 0.067$. Bubbles introduced outside the mixing layer (i.e. $y_0 > 0.10$) were hardly affected by the vortex motions over the length of our computational domain, so we are confident that the downstream concentration profiles within the mixing layer are representative of those found with bubbly flow extending across the high-speed stream (i.e. for all $y_0 > 0$).

The number of bubbles crossing unit area per unit time (i.e. the concentration flux) was calculated at downstream stations $x/L = 0.2$, 0.4, 0.6 and 0.8. Smoothed profiles of the bubble fluxes were calculated using ensemble averaging to accommodate the special initial conditions of blockwise release rather than continuous streaming. The

flux profiles presented here correspond to ensemble averaging over a streamwise interval of $\pm 0.1L$ adjoining each station. This box size was deemed acceptable because the bubbles travel an average distance of $0.2L$ between the introduction of consecutive bubbles.

The flux profiles from the simulation with $\Pi = 0$ and $\Gamma = 5$ appear on figure 14(*a*). Notice that they are antisymmetric about the centreline and possess shapes and spread rates similar to the mean velocity profiles of the single-phase mixing layer (figure 8). This self-preserving property is a classical result for passive transport, so our finding suggests that a small slip velocity ($1/\Gamma = 0.2$) does not significantly modify expectations based on passive behaviour. The profiles from our second simulation ($\Pi = 0.067$, $\Gamma = 5.0$) appear on figure 14(*b*). Notice that whilst these are also self-preserving, they are now skewed towards the high-speed stream, consistent with expectations for the effect of inertial drift in vertical downflow; recall our earlier results of §3. On the other hand, approximate self-preservation was not anticipated so this is regarded as a key finding of the present study.

6. Conclusions

Simple models of bubble motions in isolated-vortex flows have been described as an aid to understanding the role of coherent structures in mixing-layer transport of bubbles. The model results, supported by discrete-vortex simulations of the bubble trajectories, indicate that the following characteristics contribute to determine the trapping effects of large eddies in these turbulent shear flows.

First, bubbles are trapped in horizontal mixing-layer flow once the parameter $\Gamma = \Delta U/V_T$ exceeds a critical value ranging from about 10 when inertial forces are weak ($\Pi \to 0$) to about 3 when the inertial forces are comparable with buoyancy forces ($\Pi \sim 0.5$). Pairing of shear-layer vortices does not significantly affect the local bubble concentrations and it may even enhance their trapping power.

Secondly, bubbles are also trapped in vertical mixing-layer flow and the concentration profiles are skewed toward the high-speed stream in downflow when the inertial–buoyancy parameter $\Pi = \Delta U^2/2gx$ exceeds about 0.05. The effect is enhanced by lift forces due to slip motion of the bubbles in the shear flow. Because of this skewing, it is not strictly reasonable to describe the transport by a simple effective diffusivity as supposed in classical models of passive tracers. Moreover, if a diffusivity representation is sought, then the spread rate behaviour of the bubble layer demands an effective Schmidt number of about unity, a value significantly larger than that adopted to reproduce the spread rate behaviour of passive tracers. This aspect is considered further in Sene *et al.* (1993).

The discrete-vortex method has been demonstrated to provide a versatile basis for evaluating the structural-dynamic implications of Auton's force law for bubble motions in unsteady and non-uniform flows with vorticity. Our simulations have provided new insight into several key processes governing bubble transport at low concentrations and, in particular, how the transport scales on the shear-to-slip velocity ratio Γ and the inertia-to-buoyancy force ratio Π. We caution that the accuracy of the results presented here can only be checked by comparison with experimental measurements. However, we have demonstrated that they are not very sensitive to details of the assumptions made in the discrete-vortex model or the drag law adopted for the bubble motions.

Our appreciation is due to the four referees for their extensive expert guidance. This

work was undertaken at DAMTP, University of Cambridge, where K.J.S. was maintained (1981–84) by an SERC-CASE award with CERL, Leatherhead, and N.H.T. by a grant (1981–83) from Schlumberger–Doll Research, Ridgefield, Connecticut. The completion of our paper was supported by NERC, by the Wolfson Group for Flow and Mixing, Cambridge University, and by FRED Ltd, Research Park, Birmingham University.

REFERENCES

ASHURST, W. T. 1977 Numerical simulations of turbulent mixing layers. In *Turbulent Shear Flows 1*, p. 402. Springer.

ASHURST, W. T. & MEIBURG, E. 1988 Three-dimensional shear layers via vortex dynamics. *J. Fluid Mech.* **189**, 87.

AUTON, T. R. 1983 The dynamics of bubbles, drops and particles in motion in liquids. PhD thesis, University of Cambridge.

AUTON, T. R., HUNT, J. C. R. & PRUD'HOMME, M. 1988 The force exerted on a body in inviscid unsteady nonuniform rotational flow. *J. Fluid Mech.* **197**, 241.

BROWN, G. L. & ROSHKO, A. 1974 On density effects and large structure in turbulent mixing layers. *J. Fluid Mech.* **64**, 775.

CHEIN, R. & CHUNG, J. N. 1987 Effects of vortex pairing on particle dispersion in turbulent shear flow. *Intl J. Multiphase Flow* **13**, 785.

CHORIN, A. J. 1973 Numerical study of slightly viscous flow. *J. Fluid Mech.* **57**, 785.

CHUNG, J. N. & TROUTT, T. R. 1988 Simulation of particle dispersion in an axisymmetric jet. *J. Fluid Mech.* **186**, 199.

CLIFT, R., GRACE, J. R. & WEBER, M. E. 1978 *Bubbles, Drops and Particles.* Academic.

FIEDLER, H. E. 1974 Transport of heat across a plane turbulent mixing layer. *Adv. Geophys.* **18A**, 93.

GHONIEM, A. F., CHORIN, A. J. & OPPENHEIM, A. K. 1981 Numerical modelling of turbulent combustion in premixed gases. In *18th Symp. on Combustion.* The Combustion Institute.

GOLDRING, B. T., MAWER, W. T. & THOMAS, N. H. 1980 Level surges in the circulating water downshaft of large generating stations. *Proc. Third Intl Pressure Surges Conf., Coventry, UK.* BHRA.

HULIN, J.-P., FIERFORT, C. & COUDOL, R. 1982 Experimental study of vortex emission behind bluff obstacles in a gas-liquid vertical two-phase flow. *Intl J. Multiphase Flow* **8**, 475.

HUSSAIN, A. K. M. F. 1983 Coherent structures – reality and myth. *Phys. Fluids* **26**, 2816.

KIYA, M., ARIE, M. & HARIGANE, K. 1980 Numerical simulation of gross structure in turbulent mixing layers by the discrete vortex model. *Bull. JSME* **23**, 1959.

LEONARD, A. 1980 Review of vortex dynamics for flow simulation. *J. Comput. Phys.* **37**, 289.

MOORE, D. W. 1981 On the point vortex method. *SIAM J. Sci. Statist. Comput.* **2**, 65.

NIELSEN, P. 1984 On the motion of suspended sand particles. *J. Geophys. Res.* **89**, 616.

PETERS, N. & WILLIAMS, F. A. 1980 Coherent structures in turbulent combustion. In *Proc. Intl Conf. on The Role of Coherent Structures in Modelling Turbulence and Mixing, Madrid, Spain.*

SENE, K. 1985 Aspects of bubbly two-phase flow. PhD thesis, University of Cambridge.

SENE, K., THOMAS, N. H. & HUNT, J. C. R. 1993 Experimental study and diffusion modelling of bubbly mixing layers. *Intl J. Multiphase Flow* (to be submitted).

SHIBIYAMA, T. & HORIKAWA, K. 1980 Laboratory study of sediment transport mechanism due to wave action. *Proc. JSME* **296**, 131.

SOO, S. L. 1967 *Fluid Dynamics of Multiphase Systems.* Blaisdall.

SPALART, P. R. & LEONARD, A. 1981 Computation of separated flows by a vortex tracing algorithm. *AIAA 14th Fluid and Plasma Dynamics Conf., Palo Alto, California.*

THOMAS, N. H. 1982 Air demand distortion in hydraulic models. *Proc. Intl Conf. on Hydraulic Modelling of Civil Engineering Structures, Coventry, UK.* BHRA.

THOMAS, N. H., AUTON, T. R., SENE, K. & HUNT, J. C. R. 1983 Entrapment and transport of

bubbles by transient large eddies in multiphase turbulent shear flows. In *Proc. Intl Conf. on Physical Modelling of Multiphase Flows, Coventry, UK.* BHRA.

TOOBY, P. F., WICKS, G. L. & ISAACS, J. D. 1977 The motion of a small sphere in a rotating velocity field: a possible mechanism for suspending particles in turbulence. *J. Geophys. Res.* **82**, 2096.

TOWNSEND, A. A. 1976 *The Structure of Turbulent Shear Flows*, 2nd edn. Cambridge University Press.

WALLIS, G. B. 1969 *One-Dimensional Two-Phase Flow.* McGraw-Hill.

WOOD, D. H. & BRADSHAW, P. 1982 A turbulent mixing layer constrained by a solid surface. Part 1. Measurements before reaching the surface. *J. Fluid Mech.* **122**, 57.

WYGNANSKI, I. & WEISBROT, I. 1988 On the pairing process in an excited plane turbulent mixing layer. *J. Fluid Mech.* **195**, 161.